# Integrated analytical-field design method of multi-disc magnetorheological clutches for automotive applications

**Krzysztof KLUSZCZYŃSKI** [iD] **and Zbigniew PILCH**[*]

Cracow University of Technology, Faculty of Electrical and Computer Engineering, ul. Warszawska 24, 31-155, Cracow, Poland

**Abstract.** This study proposes a new integrated analytical-field design method for multi-disc magnetorheological (MR) clutches. This method includes two stages, an analytical stage (composed of 36 algebraic formulas) and a field stage based on the finite element method (FEM). The design procedure is presented systematically, step-by-step, and the results of the consecutive steps of the design calculations are depicted graphically against the background of the entire considered clutch. The essential advantage of the integrated method with this two-stage structure is the relatively high accuracy of the first analytical stage of the design procedure and the rapid convergence of the second field stage employing the FEM. The essence of the new method is the introduction of a yoke factor $k_Y$ (the concept of which is based on the theory of induction machines) that determines the ratio of the total magnetomotive force required to magnetise the entire magnetic circuit of the clutch to the magnetomotive force required to magnetise the movement region. The final value, the yoke factor $k_Y$ is determined using loop calculations. The simplicity of the developed design method predisposes its use in optimisation calculations. The proposed method can also be adapted to other MR devices analysed in shear mode.

**Key words:** electromechanical convertor; drive system component; electromagnetic calculation; MR fluids; MR multi-disc clutch; clutch design; analytical-field design.

## 1. INTRODUCTION

Recently, there has been a systematic increase in interest in the use of magnetorheological (MR) fluids with viscosity controlled by an electric signal; these fluids can be found in different types of devices, including linear dumpers [1, 2], rotary dumpers [3, 4], shock absorber [5], active suspensions [6], brakes [7–11], clutches [6, 12–14], and valves [15, 16] and seem to be especially useful in automotive and motorcycle drive systems and automotive disengagement auxiliaries [6, 7, 10, 14, 17]. Descriptions of the constructed and launched prototypes of such devices, measuring stations for testing their properties [13, 17, 18], and analytical and field methods for their modelling and design [19], including optimisation calculations [10, 19], can be found in the literature.

A promising field for the application of MR fluids can be considered to be clutches because of the ease of the coupling and decoupling process and the possibility of operating at a constant slip state. In addition, an MR clutch can act as an overload protection system [6].

The devices with MR fluids presented in the literature can be classified into different types, namely cylindrical (drum) [13, 20], disc [10], or hybrid [14]. A comparison of the different MR brake types from the viewpoint of maximum torque and constrained volume is given in [21]. For devices with a disc structure (used in brakes and clutches), the possibility of a different number of discs (from one to five) is indicated, and each number of discs is associated with different properties with respect to the overall dimensions, geometrical proportions, and values of the maximum torque per volume ratio $T_{mx}/V$, and maximum torque per mass ratio $T_{mx}/m$ [8–10]. These numerous possibilities of varying the geometrical proportions of devices and increasing the values of the above-mentioned ratios by selecting different numbers of discs appear to be a particularly promising advantage. However, they also generate the requirement to develop an effective method for designing multi-disc constructions. The design methods presented in the literature are largely based on time-consuming field calculations [7, 10, 12, 21], and the articles related to optimisation calculations do not contain information on the selection of parameters, geometrical dimensions, and winding data for the first initial variant. Articles [7, 23] are excellent examples of optimal designs that use magnetic circuit analysis.

Based on the experience related to the design of electrical machines and actuators [22, 24], different devices with smart materials (including MR linear-rotary brakes 2DoF [25], and linear actuators with shape memory alloys (SMAs) [26, 27]), the authors undertook the development of a novel integrated analytical-field method for designing multi-disc MR clutches that included two stages, namely analytical and field stages. The essential advantage of such a two-stage method is the satisfactory accuracy of the first analytical stage of the design procedure (including only 36 algebraic formulas) and the rapid con-

vergence of the second field stage of the design procedure based on the FEM.

The main view of an exemplary two-disc ($N = 2$) MR clutch (the simplest case of a multi-disc MR clutch) is illustrated in Fig. 1. Owing to its symmetry, it is sufficient to present only a quarter of the entire construction. The figure consists of three sections and indicates successively a primary member (connected to the driving motor), a secondary member (connected to the driven device), and an assemblage of both members constituting the entire device.
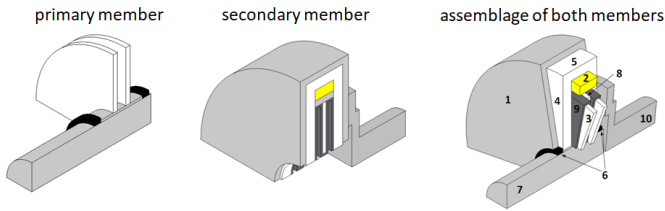


**Fig. 1.** Exemplary two-disc MR clutch ($N = 2$) – general view and introductory terminology

The numbers 1, 2, 3, ..., 10 indicate the consecutive constructional parts: 1 – non-magnetic housing, 2 – coil, 3 – discs of primary member, 4 – cover yoke, 5 – cylinder yoke, 6 – bearings, 7 – non-magnetic shaft of primary member, 8 – discs of secondary member, 9 – MR fluid gaps, 10 – non-magnetic shaft of secondary member.

Particular care must be taken to prevent the leakage of magnetorheological fluid in the coupling. It is necessary to use an appropriate sealing system, the selection of which is dictated by the operating conditions.

Note that the terminology proposed by the authors is influenced by the theory of transformers and rotating electrical machines.

## 2. DETERMINATION OF SHAFT AND DISC DIMENSIONS – BEGINNING OF ANALYTICAL STAGE OF DESIGN PROCEDURE

### 2.1. Determination of shaft radius $r_s$ and inner radius of primary member discs $r_{1i}$

The radius of a shaft $r_s$ depends mainly on the maximum value of the developed clutching torque $T_{mx}$. Clutching torque causes torsional stress in the shaft, whose maximum value divided by the torsional circular section-modulus $W_o$ must be less than or equal to the allowable stress $k_s$ for the selected type of steel.

$$\frac{T_{mx}}{W_o} \leq k_s, \tag{1}$$

where

$$W_o = \frac{\pi \cdot r_s^3}{2}. \tag{2}$$

In general, the designer introduces an additional safety factor $k_{safe}$

$$\frac{k_{safe} \cdot T_{mx}}{W_o} \leq k_s. \tag{3}$$

Consequently, the minimum shaft radius $r_{s\min}$ is determined by the following inequality resulting from equation (4):

$$r_{s\min} = \sqrt[3]{\frac{2 \cdot k_{safe} \cdot T_{mx}}{\pi \cdot k_s}}. \tag{4}$$

Knowing the value of the minimum shaft radius $r_{s\min}$, one can fit the suitable bearings (their type and size). The inner radius of the bearings $r_{bi}$ must satisfy the following inequality:

$$r_{bi} \geq r_{s\min} \tag{5}$$

and must be correlated with the list of standard bearing sizes (3.5; 4; 4.5; 5; 6; 7.5; 8.5; 10; 12.5;... mm) [28] with the appropriate tolerance.

We denote the selected radius of the shaft resulting from inequality equation (5) and from the list of standard sizes by $r_s$ (see Fig. 2a). Note that throughout this article, the following rule for marking dimensions is used in subsequent drawings: black – currently calculated dimensions, grey and dashed lines – dimensions related to completed calculations or future calculations.
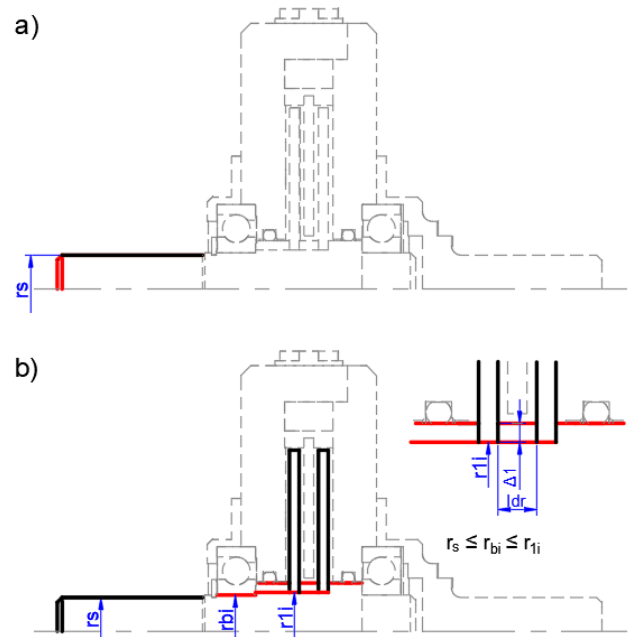


**Fig. 2.** Relationships among radii: $r_s$; $r_{bi}$, and $r_{1i}$. a) Shaft radius of MR fluid clutch $r_s$, b) inner radius of bearings $r_{bi}$ and internal radius of primary member discs $r_{1i}$

The primary member discs are placed on the shaft; their inner radius $r_{1i}$ depends on the manner in which they are mounted on the shaft. As can be observed in Fig. 2b, the inner radius of primary member discs $r_{1i}$ is marginally greater than the inner radius of bearings $r_{bi}$, and the inner radius of bearings $r_{bi}$ is marginally greater than the radius of shaft $r_s$:

$$r_s \leq r_{bi} \leq r_{1i}. \tag{6}$$

2

Bull. Pol. Acad. Sci. Tech. Sci. 69(6) 2021, e139392

These minor differences among the radii are dictated by the fine fit requirements. For further design calculations, we assume that

$$r_{1i} \cong r_{bi} \cong r_s. \tag{7}$$

For the proper positioning of the discs along the shaft, the discs must be spaced apart by distance rings with a thickness of $\Delta_1$ made of non-magnetic steel (see the inset in the upper part of Fig. 2b). The length of the distance rings $l_{dr}$ is determined at the end of the next section.

### 2.2. Choice of thickness of MR fluid gap, thickness of discs, and internal radius of secondary member discs

To select the correct thickness of the MR fluid gap $g$, two opposing criteria for different characters must be considered:

- electromagnetic criterion – ensuring the maximum value of the magnetic field in the MR fluid-gaps and consequently, the maximum value of the clutching torque;
- mechanical criterion – preventing the mechanical effect of clutch seizure.

We begin with our considerations based on the first criterion. The B-H curve for typical magnetic steel forming a ferromagnetic core is depicted in Fig. 3a and the B-H curve for MR fluid MRF-140CG is depicted in Fig. 3b [29].
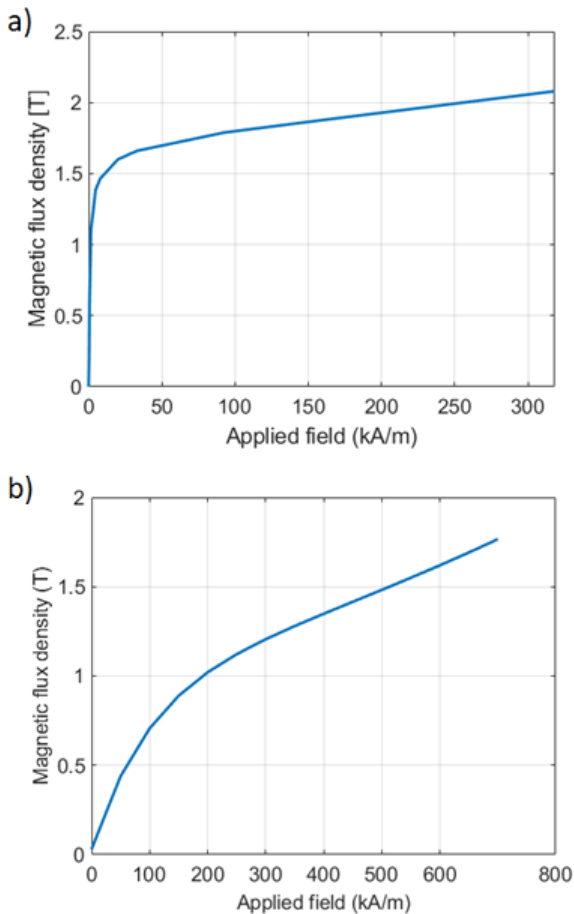


**Fig. 3.** B-H curves for magnetic steel and MR fluid MRF-140CG. a) B-H curves for ferromagnetic steel [30]; b) B-H curves for MR fluid MRF-140CG [29]

Both these curves exhibit nonlinear characteristics and include three peculiar regions, namely the linear part, knee, and saturation. The relative magnetic permeabilities of magnetic steel versus magnetic flux density for ferromagnetic steel $\mu_{Fe}$ and for MR fluid MRF-140CG $\mu_{MR}$ are depicted in Fig. 4.
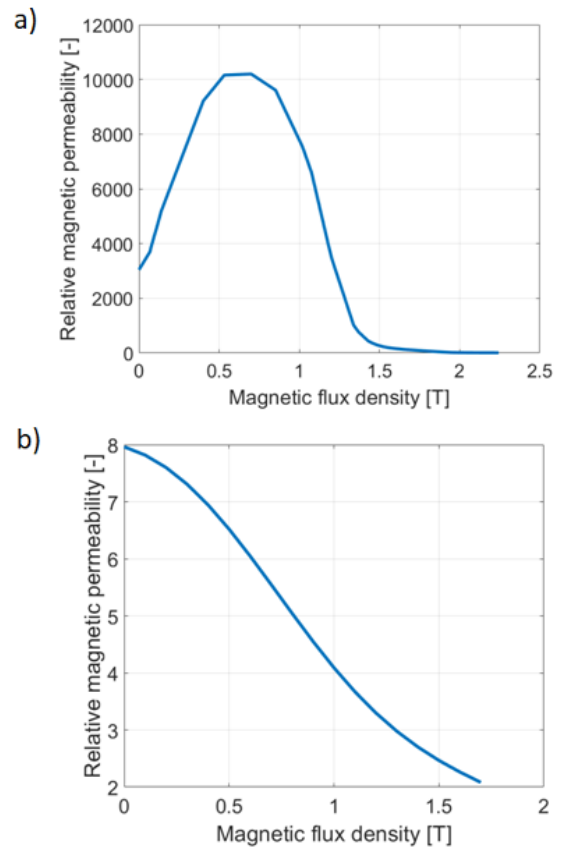


**Fig. 4.** Relative magnetic permeabilities for magnetic steel and MR fluid MRF-140CG. a) Relative magnetic permeability characteristics $\mu_{Fe}(B)$ for ferromagnetic steel [30], b) Relative magnetic permeability characteristics $\mu_{MR}(B)$ for MT fluid MRF-140CG [29]

Comparing the values of magnetic permeabilities $\mu_{Fe}$ and $\mu_{MR}$ for a magnetic flux density equal to $0.7T$ (which is the recommended value of magnetic flux density in the MR fluid gaps) [8], it can be concluded that the magnetic properties of the MR fluid are approximately 1800 times worse than those of steel. This leads to the conclusion that the thickness of the MR fluid gaps has a decisive influence on the total reluctance of the entire magnetic core, and that from the magnetic field point of view, the thickness of the gaps should be as small as possible. By minimising the MR fluid-gap thickness, the magnetic field and clutching torque are maximised (at a fixed magnetomotive force).

The second criterion imposes a large MR fluid gap. There are numerous different reasons that can lead to a seized clutch, including shaft bending, eccentricity of the shaft arrangement due to damage or natural wear of the bearings, and buckling of the discs. In all these cases, a large fluid gap reduces the risk of clutch seizing. The aforementioned problem of the proper selection of the gaps is widely known, e.g., in asyn-

Bull. Pol. Acad. Sci. Tech. Sci. 69(6) 2021, e139392

3

chronous machines, where it is related to the suitable choice of the air gap between the stator and rotor. This problem also occurs in other specific electromechanical devices, such as MR brakes and motor pumps. Based on the design experience and industrial practice relating to small and middle power induction machines [31], MR brakes [10], and motor pumps [32], it can be concluded that the recommended MR value of the MR fluid gaps should be within the range of 0.5–1 mm, i.e., $g = (0.5-1)$ mm [8, 31–33].

Returning to the multi-disc MR clutches, it is assumed that the thickness of the main MR fluid gaps $g$ among the neighbouring discs and thickness of the side-fluid gaps (also known as annular ducts [10]) are the same (there is no evident reason why their values should be differentiated). Considering the above assumption, the internal radius of the secondary member discs $r_{2i}$ can be determined as the following sum:

$$r_{2i} = r_{1i} + \Delta_1 + g, \tag{8}$$

where $g$ is the selected thickness of the MR fluid gap common to the main gaps of the discs and side gaps.

The next essential parameter is the thickness of discs $d$. It is assumed that the thickness of the primary member discs $d_1$ is equal to the thickness of the secondary member discs $d_2$; thus, $d_1 = d_2 = d$. The thickness of the discs $d$ results from the material strength calculation and requires consideration of the shaft speed, centrifugal forces, and required disc stiffness.

The length of the distance rings $l_{dr}$ between the discs is equal to the sum

$$l_{dr} = d + 2g, \tag{9}$$

as indicated in Fig. 2b.

### 2.3. Choice of working points at B-H curves and yield stress vs. magnetic field density curve

As mentioned above, the MR clutch includes two types of magnetic materials. The B-H curves for both magnetic materials, ferromagnetic steel and MR fluid, and additional curves indicating the dependence of the relative magnetic permeabilities of steel $\mu_{Fe}$ and MR fluid $\mu_{MR}$ on magnetic flux density $B$ are depicted in Fig. 3a, b and Fig. 4a, b, respectively. As can be observed in Fig. 4a, the maximum value of the magnetic permeability for steel appears in the range of 0.5–0.8 T.

Typically, the recommended value of the magnetic flux density $B_0$ in the movement region of electromechanical devices, i.e., in the air gaps of induction motors [33], fluid gaps of MR brakes, or fluid gaps of MR clutches [10, 23] is equal to $0.7T$. In a multi-disc MR clutch, the movement region consists of the MR fluid gaps and ferromagnetic discs. If the magnetic field density in the MR fluid gaps and discs is $0.7T$, then the relative magnetic permeability is approximately 10 000 in the ferromagnetic discs and approximately 5.5 in the MR fluid gaps. As can be observed, the magnetic permeability of the ferromagnetics in the movement region is approximately 1800 times greater than that in the MR fluid gaps.

In other parts of the magnetic circuit, outside the movement region, there are regions with a significantly smaller cross-section. For instance, in induction motors, these critical regions are located in the stator and rotor teeth regions, and possibly in the stator and rotor yokes. The locations of the critical regions in MR brakes and MR clutches are indicated in [7, 8] and [12], respectively. It is of utmost importance to ensure that while the magnetic induction in the movement region is equal to $B_0$, the maximum value of magnetic flux density $B_{mx}$ at the critical point of the ferromagnetic core is less than the saturation point, which is approximately $1.6T$ and is associated with the appearance of the knee on the steel B-H curve (Fig. 3a). Most frequently, designers of electromagnetic devices use values of magnetic flux density in the most saturated fragments of the magnetic circuit $B_{mx}$ at level $B_{mx} = (1.1-1.3)T$.

Next, we focus our attention on the B-H curve for the MR fluid (Fig. 3b) and on the curve presenting the relative magnetic permeability of MR fluid vs. magnetic flux density (Fig. 4b). The knee for MR fluid occurs at approximately $0.8T$. Hence, we can conclude that the selection of the magnetic flux density in the movement region at the level of $0.7T$ is fully justified from the viewpoint of the magnetic properties of the MR fluid (this value is less than the above-indicated knee at the B-H curve for the MR fluid).

The characteristics that play a key role in generating the clutching torque are the curves representing the yield stress of the MR fluid $\tau$ as a function of the magnetic flux density $B$ $\mu_{MR}$ (Fig. 5a) and as a function of the relative magnetic permeabil-
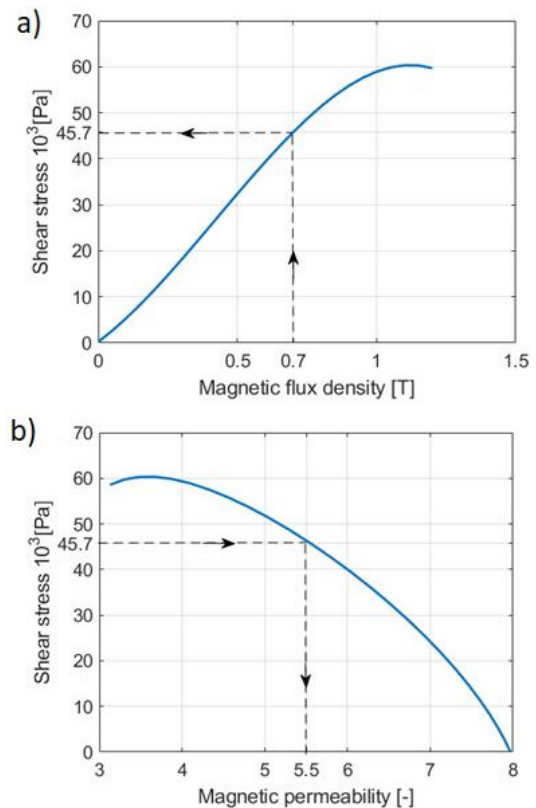


**Fig. 5.** Yield stress characteristics $\tau(B)$ and $\tau(\mu_{MR})$ for MR fluid MRF-140CG [29]. a) Yield stress characteristics $\tau(B)$ for MRF-140CG, b) Yield stress characteristics $\tau(\mu_{MR})$ for MRF-140CG – elaborated by authors on the basis in Figs. 4b and 5a

4

Bull. Pol. Acad. Sci. Tech. Sci. 69(6) 2021, e139392

ity for the MR fluid (Fig. 5b). We intend to obtain a high yield stress value $\tau_y$ (Fig. 5a) with a small decrease in the value of magnetic permeability $\mu_{MR}$ (Fig. 5b). From this point of view, the value of the magnetic flux density in the MR fluid gaps appears to be the most appropriate: $\tau_y(B_0 = 0.7T) = 45.7$ kPa, $\mu_{MR} = f^{-1}[\tau_y(B_0 = 0.7T)] = 5.55$ (Fig. 5a, b).

In summary, the selected working points for all essential curves are located in the upper part of the linear region and below the knee.

### 2.4. Clutching torque $T_c$

We determine the clutching torque $T$ acting on one side of the secondary member disc of an N-disc MR clutch under the assumption that a uniform magnetic field $B_0$ passes through the layers of the MR fluid and discs (perpendicular to their frontal surfaces) and transforms the MR fluid in the gaps into a semi-solid body with significantly increased viscosity, making the relative displacement of the discs impossible.

Such behaviour of the MR fluid is described by the Bingham model in the form of the following conditional equality [7]:

$$|\tau(\dot{\gamma}, B)| = \tau_y(B) + \eta|\dot{\gamma}| \quad \text{if} \quad \tau_y(\dot{\gamma}, B) \geq \tau(\dot{\gamma}, B), \quad (10)$$

where $\tau(\dot{\gamma}, B)$ is the total shear stress, $\tau_y(B)$ is the field-dependent yield stress, $\eta$ is the fluid viscosity, $\dot{\gamma}$ is the shear stress rate, and $\eta|\dot{\gamma}|$ is the viscous friction.

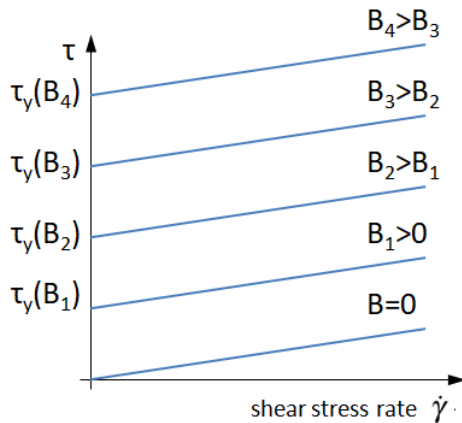The graphical interpretation of the above relation for Bingham plastics is depicted in Fig. 6.



**Fig. 6.** Bingham model – graphical representation

As can be observed, the MR fluid can resist the sheer up to a certain controllable value of yield stress $\tau_y(B)$; on exceeding this value, it behaves as a fluid. In a clutch functioning in shear mode, the primary and secondary member discs do not move relative to each other $\dot{\gamma} = 0$ and, consequently, the developed clutching torque depends only on the magnetic flux density $B$ and yield stress $\tau_y(B)$; thus, $T = f[\tau_y(B)]$.

The value of the clutching torque can be determined based on the reasoning presented below and considering Fig. 7 and Fig. 8.

These images demonstrate that the generation of the clutching torque occurs in the space between the overlapping surfaces
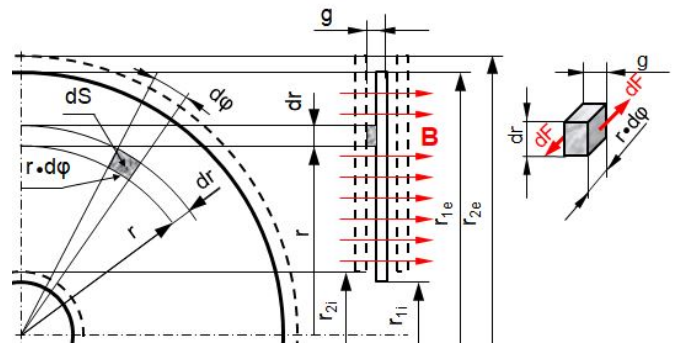


**Fig. 7.** Single disc – geometrical denotations for calculating clutching torque
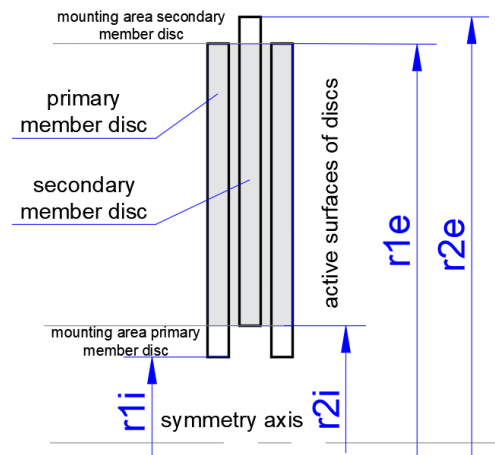


**Fig. 8.** Neighbouring discs of primary and secondary clutch members and their overlapping surfaces

of the primary and secondary member discs. These overlapping surfaces are bounded by an inner circle of radius $r_{1e}$ and outer circle of radius $r_{2i}$. In the area of the remaining non-overlapping parts of the discs, the magnetic flux density rapidly decreases and approaches zero [10, 12]. This can be observed later in the article in the figures presenting the results of the FEM calculations (Section 2.1).

In the polar coordinate system, the elementary force $dF$ and elementary torque $dT$ acting on the incremental surfaces $dS = r \cdot d\phi \cdot dr$ (where $r$ is the current radius, $d\varphi$ is the angle increment, ND $dr$ is the radius increment) can be expressed as follows:

$$dT = r \cdot dF = r \cdot \tau_y(B_0)dS = r^2 \tau_y(B_0) \cdot d\phi dr. \quad (11)$$

By integrating, one can determine the clutching torque acting on one side of the secondary member disc $T_{os}$:

$$T_{os} = \int_{r_{2i}}^{r_{1e}} \int_0^{2\pi} dT =$$

$$= \frac{\pi}{3} \cdot \tau_y(B_0) \cdot \left( r_{1e}^3 - r_{2i}^3 \right), \quad (12)$$

The N-disc MR clutch has $2N$ surfaces; therefore, the resultant torque value is ultimately equal to

$$T = \frac{4\pi}{3} \cdot N \cdot \tau_y(B_0) \cdot \left(r_{1e}^3 - r_{2i}^3\right). \tag{13}$$

Analysing the transient states of the MR clutch or considering its operation at constant slip (when primary and secondary member discs are moving relative to each other), it is necessary to consider the extended formula for torque containing a viscous torque component proportional to the relative velocity of the discs:

$$T = \frac{4\pi}{3} \cdot N \cdot \left(r_{1e}^3 - r_{2i}^3\right) \cdot \left(\tau_y(B_0) + \eta \frac{d\gamma}{dt}\right). \tag{14}$$

Note that the correctness of the simplifying assumptions referring to the uniform distribution of the magnetic field passing through the MR gaps and discs is confirmed by the FEM calculations in Section 4.1.

Assuming a uniform distribution of the magnetic field density, we can also determine the value of the magnetic flux $\Phi_0$, leaving the movement region and entering the cover and cylindrical yokes:

$$\Phi_0 = \pi B_0 \cdot \left(r_{1e}^2 - r_{2i}^2\right). \tag{15}$$

Next, we analyse equation (13). The most suitable value of magnetic flux density $B_0$ in the MR fluid gaps was selected in Section 2.3, ($B_0 = 0.7T$). The yield stress $\tau(B_0)$ can be determined from the curve in Fig. 5a ($\tau_0 = \tau(B_0) = 0.7T = 40kPa$) and the radius $r_{2i}$ was determined in Section 2.1 (equation (8)). This implies that the expression for the maximum clutching torque $T_{mx}$ is a function of two variables $T_{mx}(B_0) = f(N, r_{1e})$. It is clear that the radius $r_{1e}$ has a significant influence on the outer diameter of the entire clutch.

To select the correct number of discs N, different aspects must be considered, the most important of which is the torque density ratio (torque per volume $T_{mx}/V$, where V is the total volume of the clutch) and the limitations imposed on the outer dimensions or operating parameters of the clutch specified by the user based on the planned or expected application (e.g., outer length, outer diameter, total clutch volume, total clutch mass, and total inertia moment of the rotating part). All the above-mentioned dimensions or parameters are obtained at the end of the entire design process.

The introductory selected number of discs is typically a compromise between the volume (mass) of the clutch that decreases with the number of discs and the technological complexity of the clutch, which increases with the number of discs. This problem was considered in detail in [8, 12, 34]. The number of discs recommended in these studies was two ($N = 2$) or three ($N = 3$). Following the introductory selection of the number of discs, one can continue with further design calculations.

The external radius of the primary member discs $r_{1e}$ can be determined based on the following formula resulting from equation (16):

$$r_{1e} = \sqrt[3]{\frac{3T_{mx}}{4\pi N \tau_y(B_0)} - r_{2i}^3}. \tag{16}$$

As can be observed in Fig. 9, the external radius of secondary member discs $r_{2e}$ is, in relation to the external radius of primary member discs $r_{1e}$, increased by the thickness of the MR fluid gap $g$ and depth $s$ of the mounting socket made in a non-magnetic ring with a thickness of $\Delta_2$ (its purpose is to separate the movement region from the coil).
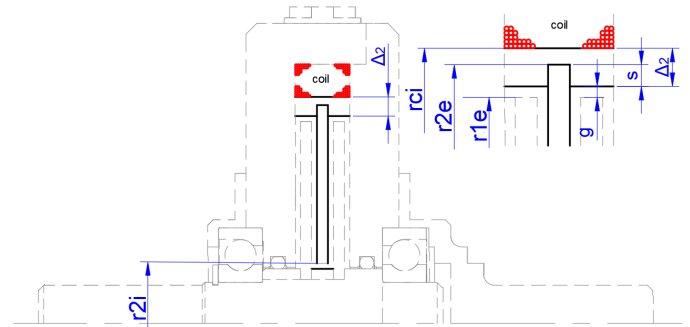
$$r_{2e} = r_{1e} + g + s \tag{17}$$



**Fig. 9.** Non-magnetic separating ring – geometrical denotation

## 3. DETERMINATION OF COIL WINDING DATA, COIL DIMENSIONS, AND YOKE DIMENSIONS ASSUMING KNOWLEDGE OF YOKE FACTOR – FURTHER ANALYTICAL STAGE OF DESIGN PROCEDURE

**3.1. Determination of required magnetomotive force (MMF)**
The magnetic flux produced by the current $I$ flowing in the coil composed of $z$ turns (magneto motive force $\Theta$ equals $I \cdot z$) passes through the $2N$ fluid gaps, $(2N - 1)$ ferromagnetic discs, two ferromagnetic cover yokes, and cylindrical yoke (Figs. 1, 2, 11).

The magnetomotive force can be divided into two components: magnetomotive force $\Theta_{mr}$ associated with the movement region composed of the MR fluid gaps and discs, and the magnetomotive force $\Theta_Y$ connected with the remaining parts of the magnetic circuit composed of two cover yokes and a cylinder yoke (these parts are required for closing the path for the magnetic flux).

$$\Theta = \Theta_{mr} + \Theta_Y. \tag{18}$$

The former component $\Theta_{mr}$ is dominant; its value can be determined based on the calculated geometrical dimensions and the selected value of the magnetic flux density $B_0$ ($B_0 = 0,7T$).

$$\Theta_{mr} = \underbrace{2Ng \cdot \frac{B_0}{\mu_0 \mu_{MR}(B_0)}}_{\Theta_{mr}(MR)} + \underbrace{(2N-1)d \cdot \frac{B_0}{\mu_0 \mu_{Fe}(B_0)}}_{\Theta_{mr}(Fe)}, \tag{19}$$

where $\Theta_{mr(MR)}$ is the magnetomotive force associated with the MR fluid gaps, $\Theta_{mr(Fe)}$ is the magnetomotive force associated with the discs, $\mu_{MR}(B_0)$ is determined from the curves in Fig. 4b, and $\mu_{Fe}(B_0)$ is determined from the curve in Fig. 4a.

6

Bull. Pol. Acad. Sci. Tech. Sci. 69(6) 2021, e139392

As indicated earlier in Section 2.3, the magnetic properties of the MR fluid are approximately 1800 times worse than those of steel. Consequently, the MMF drop across the ferromagnetic discs is hundreds of times less than that across the MR fluid gaps:

$$\Theta_{mr(Fe)} \ll \Theta_{mr(MR)}, \tag{20}$$

which implies that its value can be neglected in further design calculations:

$$\Theta_{mr} \approx \Theta_{mr(MR)}. \tag{21}$$

As previously mentioned, magnetomotive force $\Theta_Y$ is required to set up the magnetic flux in the two cover yokes and one cylindrical yoke. It is convenient to assume its value with respect to the MMF drop $\Theta_{mr}$ in the form of a ratio, which is referred to as the yoke factor $k_Y$:

$$k_Y = \frac{\Theta_{mr} + \Theta_Y}{\Theta_{mr}}. \tag{22}$$

It is worth mentioning that the proposed yoke factor $k_Y$ corresponds to the so-called saturation factor used in designing of induction motors. For properly designed electromechanical convertors its value should by in the range 1.1–1.3 (recommended values are given in books devoted to design of electrical apparatus e.g. in [35]). It results from the fact that magnetic energy stored in the movement region participates in electromechanical conversion of electrical energy into mechanical energy, whereas magnetic energy stored in the yokes does not participate in this conversion process (yokes are required for closing path for magnetic flux $\Phi_0$).

Assuming the introductory value $k_Y$ (the recommended initial value of the yoke factor $k_Y$ for the first analytical stage of the calculations ($i = 0$) is $k_Y = 1.1 - 1.2$), we can continue the design calculations. The total MMF required to set up the desired magnetic flux $\Phi_0$ (equation (15)) in the entire magnetic circuit is equal to

$$\Theta = k_Y \cdot \Theta_{mr} = \frac{\Theta_{mr} + \Theta_Y}{\Theta_{mr}} \cdot \Theta_{mr}, \tag{23}$$

where $\Theta_{mr}$ is the value known at this stage of design (see equation (19))and $k_Y$ is the introductory assumed value of the yoke factor (the initial point for the calculation loop depicted in Fig. 13).

### 3.2. Coil design

Next, we consider the coil design. As indicated in Section 2.4, the movement region is separated from the coil by a non-magnetic steel ring with a thickness of $\Delta_2$ (Fig. 9). Hence, the inner diameter of coil $r_{ci}$ is determined by the following sum:

$$r_{ci} = r_{1e} + g + \Delta_2. \tag{24}$$

The coil is wound on a carcass with a thickness of $\Delta_3$. The carcass is considered part of the coil (Fig. 10).
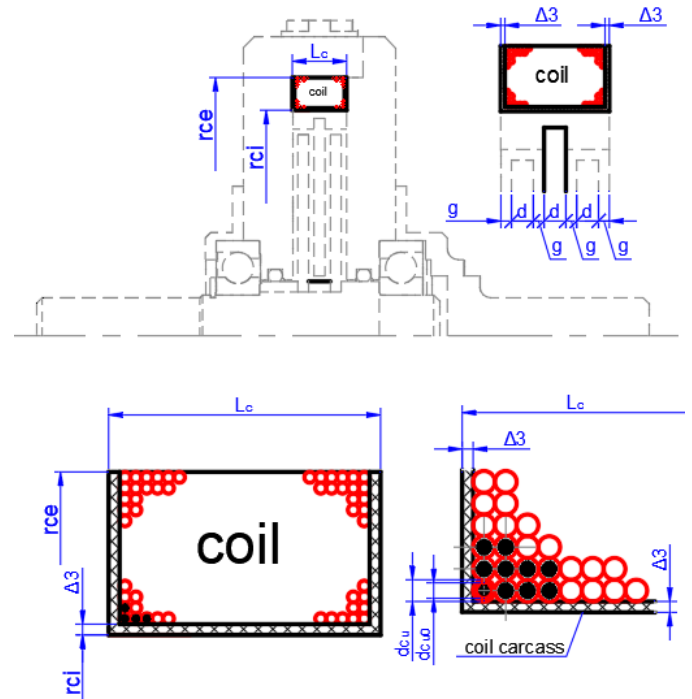


**Fig. 10.** Dimensions of coil. a) Outer dimensions of coil: $L_c$, $r_{ci}$, and $r_{ce}$. b) Layers and conductors of coil

Regarding the length of the coil $L_c$ (composed of conductors and carcass), its value depends on the number of MR fluid gaps and discs (Fig. 10).

$$L_c = [N + (N-1)] \cdot d + 2Ng = (2N-1) \cdot d + 2Ng. \tag{25}$$

Typically, the approximate value of the excitation current $I^*$ feeding the coil is known; its value results from the properties of the supply system. The current density in the coil must be selected such that a satisfactory efficiency can be obtained without excessive temperature increase. Assuming that the allowable current density for the given insulation class of wound wires is $j_{cu}^* = 4.5 \, \text{A/mm}^2$, one can calculate the values of cross-sectional area $S_{cu}^*$ and diameter of a bare conductor $d_{cu}^*$.

$$S_{cu}^* = \frac{I^*}{j_{cu}^*}, \qquad d_{cu}^* = \sqrt[2]{\frac{4 \cdot S_{cu}^*}{\pi}}. \tag{26}$$

The nominal cross-sections and diameters of the bare conductors $S_{cu0}$ and $d_{cu0}$, and the insulated conductors $S_{cu}$ and $d_{cu}$ that are used to wind the coil can be found in the AWG International Standard Specification [36]. These are the closest values greater than $S_{cu}^*$ and $d_{cu}^*$.

The corrected value of supplying current $I^*$ is determined by the formula

$$I^* = S_{cu} \cdot j_{cu}^*. \tag{27}$$

Using the value of the total MMF (equation (23)) and current $I^*$, one can easily calculate the desirable number of turns $z^*$ from the following relation:

$$z^* = \frac{\Theta}{I^*}, \tag{28}$$

Bull. Pol. Acad. Sci. Tech. Sci. 69(6) 2021, e139392

7

where $\Theta$ is the assumed MMF resulting from equations (18) and (23).

In general, $z^*$ is not an integer. Rounding the number $z^*$ to an integer number

$$z = \text{int}(z^*) + 1, \qquad (29)$$

it is necessary to marginally correct the excitation current and current density

$$I = \frac{I^* \cdot \text{int}(z^*)}{z^*}, \qquad j = \frac{I}{S_{Cu0}}. \qquad (30)$$

In the next step, we can specify the number of turns per layer of coil $n$ and number of layers $m$ that make up the coil (Fig. 10):

$$n = \text{int}\left[\frac{L_c - 2\Delta_3}{d_{Cu}}\right], \qquad (31)$$

$$m = \text{int}\left[\frac{z}{n}\right] + 1. \qquad (32)$$

Knowledge of the above values enables us to calculate the external radius of the coil $r_{ce}$ (Fig. 10).

$$r_{ce} = r_{ci} + \Delta_3 + m \cdot d_{Cu}. \qquad (33)$$

### 3.3. Determination of yoke dimensions

The clutch yoke consists of two parts: a cover yoke (Fig. 11a) and cylindrical yoke (Fig. 11b). We denote the thickness of the cover yoke by $Y'$ and its inner and external radii by $r_{Y'i}$ and $r_{Y'e}$, respectively. Similarly, the thickness of the cylindrical yoke is denoted by $Y''$ and its inner and external radii by $r_{Y''i}$ and $r_{Y''e}$, respectively (Fig. 11b).

To minimise the value of the MMF drop across yokes, it is important that the magnetic flux density at each yoke point is correspondingly lesser than the saturation point, which is approximately $1.6T$ (Fig. 3a). The detailed considerations of the spatial distribution of the magnetic flux density along the "average magnetic path" are presented in [12]. In this paper, as well as in [7], it is demonstrated that the most saturated point lies within the cover yoke at a length approximately equal to the sum

$$r_{Bmx} \cong r_{1e} + g. \qquad (34)$$

Hence, the aforementioned requirement that the magnetic flux density at each point of the yokes be lesser than the assumed maximum value $B_{mx}$ (typically $B_{mx} = (1.1-1.3T)$) can be replaced by the condition that the maximum magnetic flux density at the most saturated point of the cover yoke must be lesser than $B_{mx}$.

This enables us to determine the thickness of the cover yoke $Y'$ (Fig. 11a and Eqs. (23) and (34)).

$$Y' = \frac{\Phi_0}{2\pi \cdot r_{Bmx} \cdot B_{mx}}. \qquad (35)$$

For the cylinder yoke thickness $Y''$, there is no reason for differentiating the thickness of cover yoke $Y'$ from that of

the cylindrical yoke $Y''$. Hence, it is typically assumed that (Fig. 11b)

$$Y' = Y''. \qquad (36)$$

Considering equation (36) and based on Figs. 2b and 10, we have $r_{Y'i} = r_{1i} + \Delta_1$, $r_{Y'e} = r_{Y''e} = r_{ce} + Y'$, $r_{Y'i} = r_{ce}$, and $L_{Y''} = L_c$.
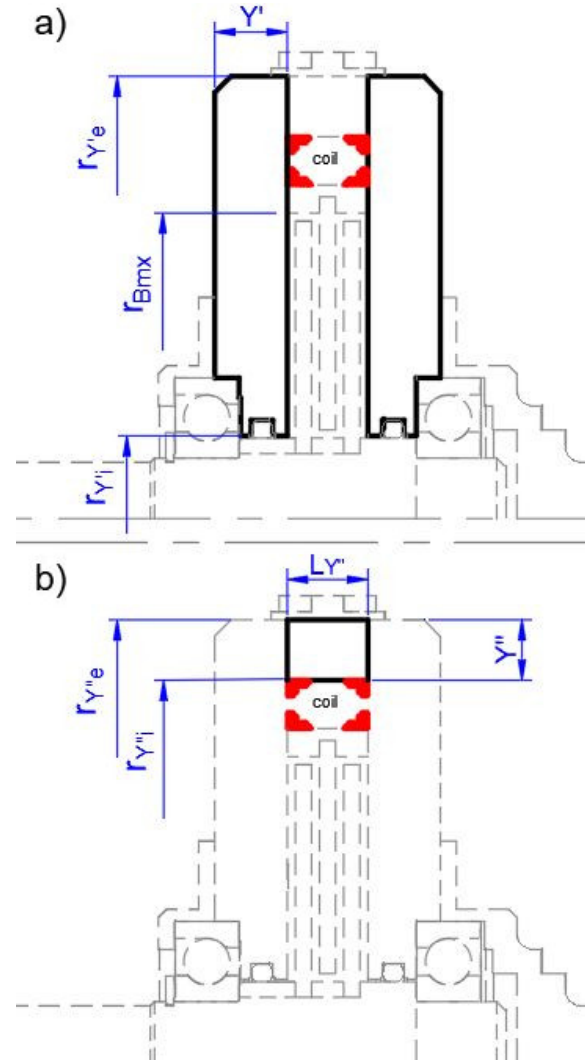


**Fig. 11.** Cover and cylindrical yoke for clutch. a) Cover yoke dimensions. b) Cylindrical yoke dimensions

At this point, we have completed the analytical stage of the design method, which has allowed us to determine all geometrical dimensions of the clutch and winding data of the coil, assuming the knowledge of the yoke factor $k_Y$.

The input (given) geometrical dimensions, factors and curves, calculated or selected geometrical dimensions, and other data referred to "Shaft, discs & rings" and "Coil & magnetic circuit (movement region and yoke)" are listed in Fig. 12 in tabular form in the order of their appearance in the text. With the specific values of the above quantities and parameters, one can develop an FEM model of the desired clutch.

8

Bull. Pol. Acad. Sci. Tech. Sci. 69(6) 2021, e139392

| | | Input Quantities | Minor dimensions | Major data | Materials factor | Loop factor | Tables & curves | Dimensions | Quantities | Units | Equations & figures |
|---|---|---|---|---|---|---|---|---|---|---|---|
| **Shaft, discs & rings** | maximum torque | $T_{mx}$ | | | | | | | | Nm | |
| | safety factor | | | | $k_{safe}$ | | | | | - | |
| | allowable stress | | | | $k_s$ | | | | | - | |
| | shaft radius/ inner radius of primary member discs | | | | | | | $r_s, r_{1i}$ | | mm | (4) |
| | inner radius of bearings | | | | | | | $r_{bi}$ | | mm | (5) |
| | outer radius of bearings | | | | | | $r_{be}$ | | | mm | |
| | inner radius of primary member discs | | | | | | | $r_{1i}$ | | mm | |
| | thickness of distance rings | | $\Delta_1$ | | | | | | | mm | |
| | length of distance rings | | | | | | | $l_{dr}$ | | mm | (9) |
| | thickness of primary and secondary member discs | | | d | | | | | | mm | |
| | number of discs | | | N | | | | | | - | |
| | external radius of primary member discs | | | | | | | $r_{1e}$ | | mm | (16) |
| | thickness of non-magnetic rings | | $\Delta_2$ | | | | | | | mm | |
| | Depth of mounting socket | | s | | | | | | | mm | |
| | external radius of secondary member discs | | | | | | | $r_{2e}$ | | mm | (17) |
| | internal radius of secondary member discs | | | | | | | $r_{2i}$ | | mm | (8) |
| **Coil & magnetic circuit (movement region and yokes)** | B-H curve for magnetic steel | | | | | | | | | | |
| | B-H curve for MR fluid | | | | | | | | | | |
| | magnetic permeability characteristics for steel | | | | | | $\mu_{Fe}=f(B)$ | | | - | Fig. 4a |
| | magnetic permeability characteristics of MR fluid | | | | | | $\mu_{MR}=f(B)$ | | | - | Fig. 4b |
| | yield stress characteristics for MR fluid | | | | | | $\tau_y=f(B)$ | | | Pa | Fig. 4 |
| | thickness of MR fluid-gap | | | g | | | | | | mm | |
| | magnetic field density in MR fluid-gaps | | | | | | | | B | T | |
| | MMF in movement region | | | | | | | | $\Theta_{mr}$ | Tm | (19) |
| | yoke factor | | | | | | | | $k_Y$ | - | (22) |
| | total MMF | | | | | | | | $\Theta$ | | (18) |
| | inner diameter of coil | | | | | | | $r_{ci}$ | | mm | (24) |
| | thickness of carcass | | $\Delta_3$ | | | | | | | mm | |
| | excitation current | I | | | | | | | | A | (27) |
| | current density | $j_{cu}$ | | | | | | | | A/mm² | (30) |
| | diameter of bare conductor | | | | | | | $d_{cu0}$ | | mm² | |
| | diameter of insulated conductor | | | | | | | $d_{cu}$ | | mm² | (26) |
| | number of coil turns | | | | | | | z | | - | (29) |
| | number of turns per one layer | | | | | | | n | | - | (31) |
| | number of layers | | | | | | | m | | - | (32) |
| | length of coil | | | | | | | $L_c$ | | mm | (25) |
| | external radius of coil | | | | | | | $r_{ce}$ | | mm | (33) |
| | max. magnetic flux density | $B_{mx}$ | | | | | | | | T | |
| | thickness of cover (cylinder) yoke | | | | | | | Y' | | mm | (35) |

**Fig. 12.** List of quantities, dimensions, parameters, and factors used

## 4. ELABORATION OF FEM MODEL FOR EXEMPLARY CLUTCH – FIELD STAGE OF DESIGN PROCEDURE

### 4.1. Sample design: two-disc MR clutch

We design a two-disc MR clutch (i.e., the simplest case of a multi-disc MR clutch: $N = 2$) developing maximum torque $T = 20$ Nm (Variant 1) and $T = 50$ Nm (Variant 2). It is assumed that the magnetic flux density in the MR fluid gaps is $B_0 = 0.7T$ (see Section 2.3) and the value of the most saturated point of the clutch (lying within the cover yoke) is equal to $B_{mx} = 1.2T$ (see Section 3.3). The coil is supplied by the excitation current $I^* = 0.6$ A, and the value of the allowable current density in the coil is $j^* = 4.5$ A/mm².

Based on mechanical considerations, it was assumed that the thickness of the discs should be $d = 2$ mm (Variant 1) and $d = 3$ mm (Variant 2), and the thickness of the MR fluid layers $g = 1$ mm (the same value for Variants 1 and 2). The remaining mechanical and material parameters are as follows: $\Delta_1 = 3$ mm, $\Delta_2 = 3$ mm, $s = 2$ mm, $\Delta_3 = 4$ mm, $k_{safe} = 1.2$, and $k_s = 75 \cdot 10^6$ Pa (for non-magnetic steel).

The required curves, B-H for magnetic steel and MR fluid MRF-140CG, relative magnetic permeability vs. magnetic flux density for magnetic steel $\mu_{Fe}$ and MR fluid MRF-140CG $\mu_{MR}$, and yield stress vs. magnetic flux density characteristics $\tau(B)$ for MR fluid MRF-140CG are depicted in Figs. 3a, b, Figs. 4a, b, and Fig. 5a, respectively.

The specifications for the bearings and conductors are included in the manufacturers' catalogues (see Sections 2.1 and 3.2).

The choice of the initial value of yoke factor $k_Y$ is of key importance for the preliminary clutch calculations. It was assumed that the initial value of the yoke factor was equal to $k_Y = 1.4$ (Case I) and $k_Y = 1.1$ (Case II). Verification of the correctness of the assumed values of the yoke factor $k_Y$ are performed using the FEM method in accordance with the scheme block presented in Fig. 13 describing the analytical-field design method.

The results of the preliminary calculations based on the analytical stage of the design procedure (the top of the scheme block in Fig. 13) for the initially assumed value of yoke factor $k_Y = 1.4$ (Case I) and $k_Y = 1.1$ (Case II) for both variants: $T = 20$ Nm (Variant 1) and $T = 50$ Nm (Variant 2) are depicted in Fig. 14 in tabular form. These results are divided into two portions: "Results independent of yoke factor $k_Y$" and "Results dependent on yoke factor $k_Y$". With this division, the results of the analytical calculations are presented in the above-mentioned table (Fig. 14).

For the "Field stage of design procedure" (the bottom of the scheme block in Fig. 13), the authors employed, for the FEM calculations, open-access program Agros2D elaborated at the Pilzen University of Technology [30] (all scripts were written in PythonLAB language). Mesh axisymmetric models of the clutches for the preliminarily calculated dimensions given in Fig. 14 for Variant 1 (Case I: $k_Y = 1.4$) and Variant 2 (Case II: $k_Y = 1.4$) are depicted in Fig. 15ab (owing to symmetry, it is sufficient to consider only half of the cross-section).

Figures 16a and 16b depict the simulation results: spatial distribution of magnitude $|B|$ of the magnetic flux density $B$ for clutch $T = 20Nm$ (Variant 1, Case I: $k_Y = 1.4$) and clutch $T = 50$ Nm (Variant 2, Case II: $k_Y = 1.4$) obtained using the Agros2D program.

The values of the magnetic flux density in the middle of the movement region (the point denoted in Fig. 16 by the drop in red) are determined from the FEM models and equal
$B_0^* = 0.7560$ T for Variant 1, Case I (Fig. 16a);
$B_0^* = 0.6672$ T Variant 1, Case II;
$B_0^* = 0.7558$ T for Variant 2, Case I (Fig. 16b);
$B_0^* = 0.6659$ T Variant 2, Case II.

These values differ from the introductory assumed value $B_0 = 0.7T$. This implies that it is necessary to repeat the part of "Analytical stage of design procedure" embraced by "Iteration
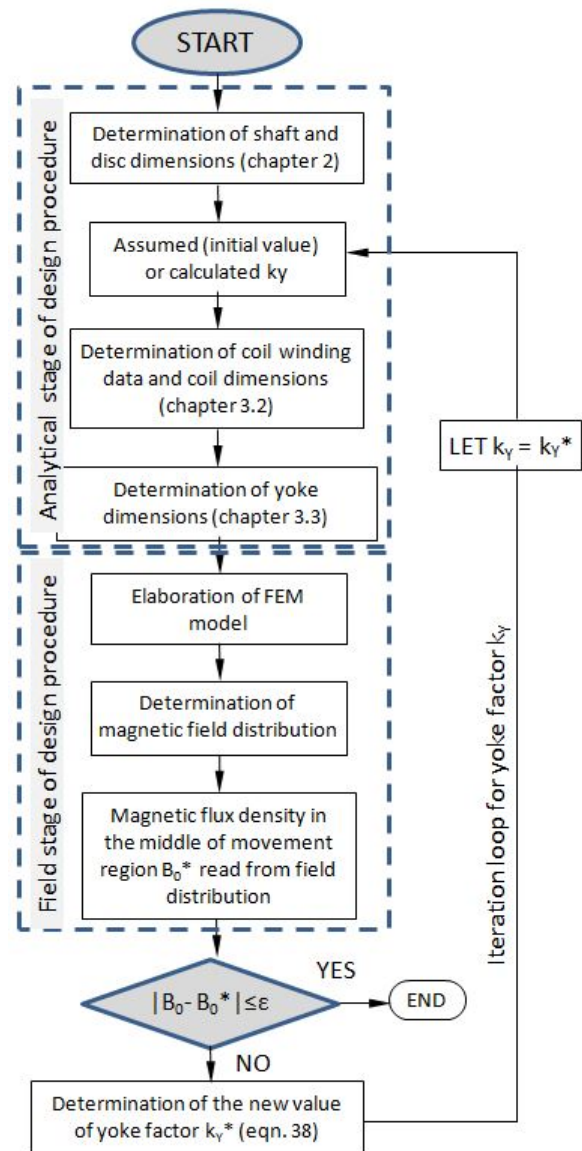


**Fig. 13.** Scheme block for analytical-field design method

| | | | Variant 1 | | Variant 2 | |
|---|---|---|---|---|---|---|
| | | | Case I | Case II | Case I | Case II |
| Results independent of yoke factor $k_Y$ | shaft radius/inner radius of primary member discs | $r_s$, $r_{1i}$ | 5.88 | 5.88 | 7.98 | 7.98 |
| | length of distance rings | $l_{dr}$ | 4 | 4 | 5 | 5 |
| | external radius of primary member discs | $r_{1e}$ | 37.05 | 37.05 | 50.4 | 50.4 |
| | external radius of secondary member discs | $r_{2e}$ | 40.05 | 40.05 | 53.4 | 53.4 |
| | MMF in movement region | $\Theta_{mr}$ | 347.26 | 347.26 | 347.26 | 347.26 |
| | inner radius of coil | $r_{ci}$ | 42.05 | 42.05 | 55.4 | 55.4 |
| | diameter of bare conductor | $d_{cu0}$ | 0.45 | 0.45 | 0.45 | 0.45 |
| | diameter of insulated conductor | $d_{cu}$ | 0.51 | 0.51 | 0.51 | 0.51 |
| | number of turns per one layer | $n$ | 18 | 18 | 23 | 23 |
| | length of coil | $L_c$ | 10 | 10 | 13 | 13 |
| | thickness of cover (cylinder) yoke | $Y'$ | 9.6 | 9.6 | 13.4 | 13.4 |
| Results dependent on yoke factor $k_Y$ | yoke factor | $k_Y$ | 1.4 | 1.1 | 1.4 | 1.1 |
| | total MMF | $\Theta$ | 486.17 | 381.99 | 486.17 | 381.99 |
| | number of layers | $m$ | 46 | 36 | 36 | 28 |
| | number of coil turns | $z$ | 810 | 637 | 810 | 637 |
| | external radius of coil | $r_{ce}$ | 65.9 | 60.8 | 74.2 | 70.1 |
| | excitation current | $I$ | 0.599 | 0.599 | 0.599 | 0.599 |

**Fig. 14.** Results of preliminary calculations based on analytical stage of design procedure

10

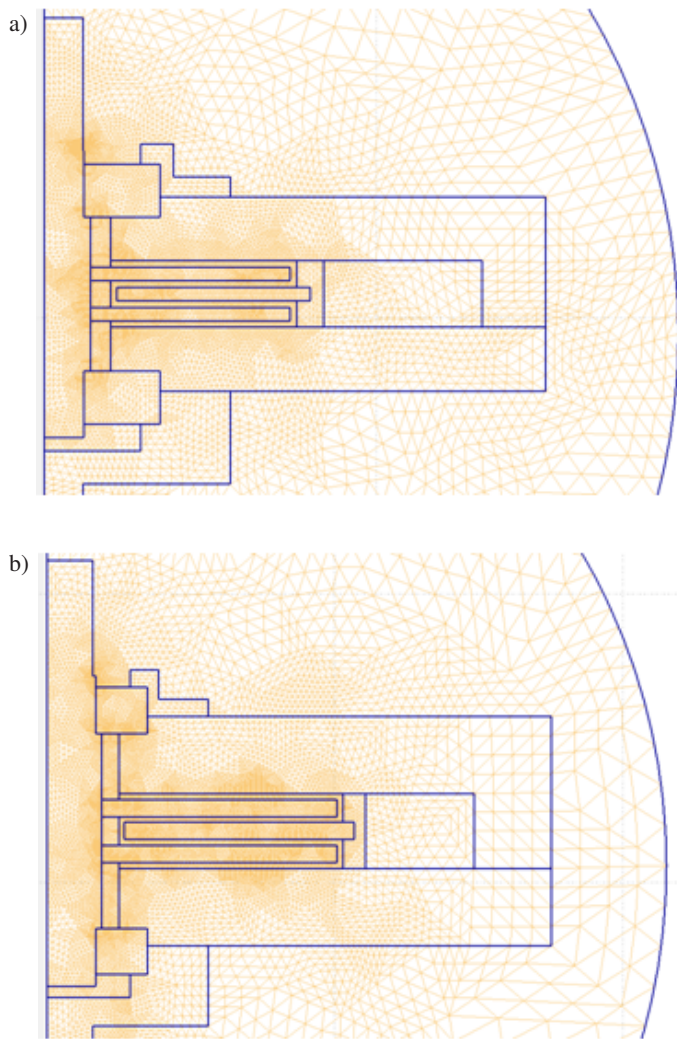Bull. Pol. Acad. Sci. Tech. Sci. 69(6) 2021, e139392

a)



b)



**Fig. 15.** Mesh models for Variant 1 ($T = 20$ Nm) and Variant 2 ($T = 50$ Nm). a) Mesh model – Variant 1 (Case I: $k_Y = 1.4$.) b) Mesh model – Variant 2 (Case I: $k_Y = 1.4$), (number of elements: 21456, DOF 42725)

loop for yoke factor $k_Y$" (Fig. 13) for the new value $k_Y^*$ resulting from the following proportion (the proportion is valid under the assumption of linearity of both B-H curves in the neighbourhood of the considered working point):

$$k_Y \cdot \Theta_{mr} - B_0^*,$$
$$k_Y^* \cdot \Theta_{mr} - B_0.$$
(37)

The new value of yoke factor $k_Y^*$ is equal to

$$k_Y^* = k_Y \cdot \frac{B_0}{B_0^*} = k_Y \cdot \frac{0.7}{B_0^*}.$$
(38)

Loop calculations must be repeated until the difference $|B_0 - B_0^*|$ becomes less than the assumed percentage accuracy $\varepsilon$ (in the sample design, it was assumed that $\varepsilon = 0.2\%$).

$$\frac{|B_0 - B_0^*|}{B_0} \cdot 100\% < \varepsilon.$$
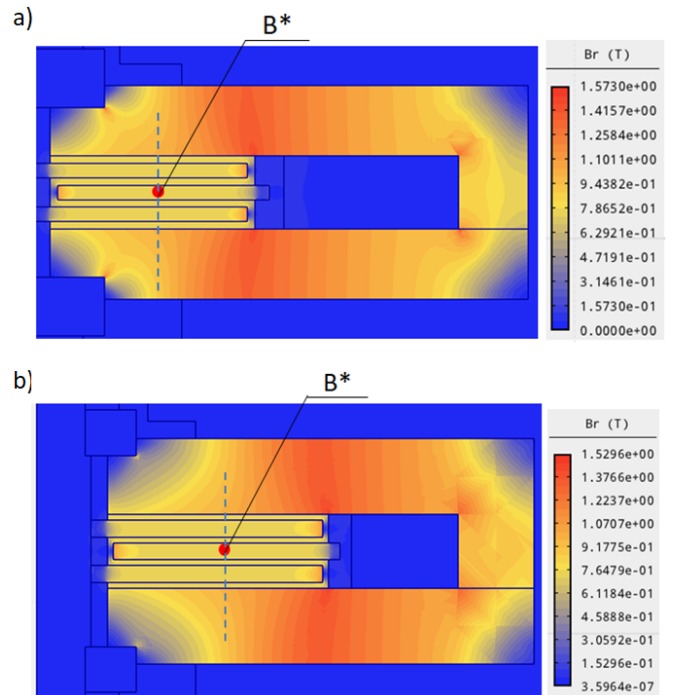(39)

a)



b)



**Fig. 16.** Spatial distribution of magnetic flux density. a) Variant 1 ($T = 20$ Nm) and b) Variant 2 ($T = 50$ Nm). a) Variant 1 (Case I: $k_Y = 1.4$). b) Variant 2 (Case I: $k_Y = 1.4$)

The results of the loop calculations for "Field stage of design procedure" for consecutive iterations for both variants of the clutch, Variant 1 and Variant 2, and for both cases, Case I and Case II, are presented in Tables 1, 2, 3, and 4, and are illustrated in Figs. 17 and 18 (Variant 1) and Figs. 19 and 20 (Variant 2).

**Table 1**
Results obtained in loop calculations for $T = 20$ Nm, $k_Y = 1.4$

| $i$ | $B_0^*$ [T] | $\varepsilon$ [%] | $k_Y^*$ [–] | $I$ [A] | $T_{mx}$ [Nm] | $z$ [–] | $m$ [–] | $r_{ce}$ [mm] |
|---|---|---|---|---|---|---|---|---|
| 0 | 0.756 | 8.01 | 1.400 | 0.599 | 20.915 | 811 | 46 | 65.9 |
| 1 | 0.730 | 4.28 | 1.296 | 0.599 | 20.279 | 751 | 42 | 63.9 |
| 2 | 0.715 | 2.10 | 1.243 | 0.599 | 19.897 | 720 | 41 | 63.4 |
| 3 | 0.707 | 0.99 | 1.217 | 0.599 | 19.697 | 705 | 40 | 62.9 |
| 4 | 0,703 | 0.46 | 1.205 | 0.599 | 19.601 | 698 | 39 | 62.3 |
| 5 | 0,701 | 0.21 | 1.200 | 0.599 | 19.556 | 695 | 39 | 62.3 |
| 6 | 0.701 | 0.09 | 1.197 | 0.599 | 19.535 | 694 | 39 | 62.3 |

**Table 2**
Results obtained in loop calculations for $T = 20Nm$, $k_Y = 1.1$

| $i$ | $B_0^*$ [T] | $\varepsilon$ [%] | $k_Y^*$ [–] | $I$ [A] | $T_{mx}$ [Nm] | $z$ [–] | $m$ [–] | $r_{ce}$ [mm] |
|---|---|---|---|---|---|---|---|---|
| 0 | 0.667 | 4.68 | 1.1 | 0.599 | 18.649 | 637 | 36 | 60.8 |
| 1 | 0.686 | 1.98 | 1.154 | 0.599 | 19.156 | 668 | 38 | 61.8 |
| 2 | 0.694 | 0.85 | 1.177 | 0.599 | 19.363 | 682 | 38 | 61.8 |
| 3 | 0.697 | 0.38 | 1.187 | 0.599 | 19.449 | 688 | 39 | 62.3 |
| 4 | 0.699 | 0.17 | 1.191 | 0.599 | 19.488 | 690 | 39 | 62.3 |

**Table 3**

Results obtained in loop calculations for $T = 50$ Nm, $k_Y = 1.4$

| $i$ | $B_0^*$ [T] | $\varepsilon$ [%] | $k_Y^*$ [–] | $I$ [A] | $T_{mx}$ [Nm] | $z$ [–] | $m$ [–] | $r_{ce}$ [mm] |
|---|---|---|---|---|---|---|---|---|
| 0 | 0.756 | 7.98 | 1.400 | 0.599 | 52.19 | 811 | 36 | 74.2 |
| 1 | 0.729 | 4.21 | 1.296 | 0.599 | 50.63 | 751 | 33 | 72.6 |
| 2 | 0.714 | 2.02 | 1.244 | 0.599 | 49.69 | 721 | 32 | 72.1 |
| 3 | 0.706 | 0.93 | 1.219 | 0.599 | 49.21 | 706 | 31 | 71.6 |
| 4 | 0.703 | 0.42 | 1.208 | 0.599 | 48.99 | 700 | 31 | 71.6 |
| 5 | 0.701 | 0.19 | 1.203 | 0.599 | 48.88 | 697 | 31 | 71.6 |

**Table 4**

Results obtained in loop calculations for $T = 50$ Nm, $k_Y = 1.1$

| $i$ | $B_0^*$ [T] | $\varepsilon$ [%] | $k_Y^*$ [–] | $I$ [A] | $T_{mx}$ [Nm] | $z$ [–] | $m$ [–] | $r_{ce}$ [mm] |
|---|---|---|---|---|---|---|---|---|
| 0 | 0.666 | 4.87 | 1.100 | 0.599 | 46.585 | 637 | 28 | 70.1 |
| 1 | 0.686 | 2.05 | 1.156 | 0.599 | 47.879 | 670 | 30 | 71.1 |
| 2 | 0.694 | 0.88 | 1.180 | 0.599 | 48.407 | 684 | 30 | 71.1 |
| 3 | 0.697 | 0.39 | 1.190 | 0.599 | 48.625 | 690 | 31 | 71.6 |
| 4 | 0.699 | 0.17 | 1.195 | 0.599 | 48.723 | 692 | 31 | 71.6 |

As can be observed, the results of the loop calculations are monotonically and rapidly convergent.

The "Analytical stage of design procedure" (the first row in Tables 1–4 denoted as $i = 0$) enables us to determine the intro-ductory dimensions and data for the clutch with the assumed values of magnetic flux density in the working region $B_0$ and maximum torque $T_{mx}$ with accuracies of (4–8)% for $B_0$ and (4–7)% for $T_{mx}$ (depending on the designer's experience in selecting the initial value of the yoke factor). The "Field stage of
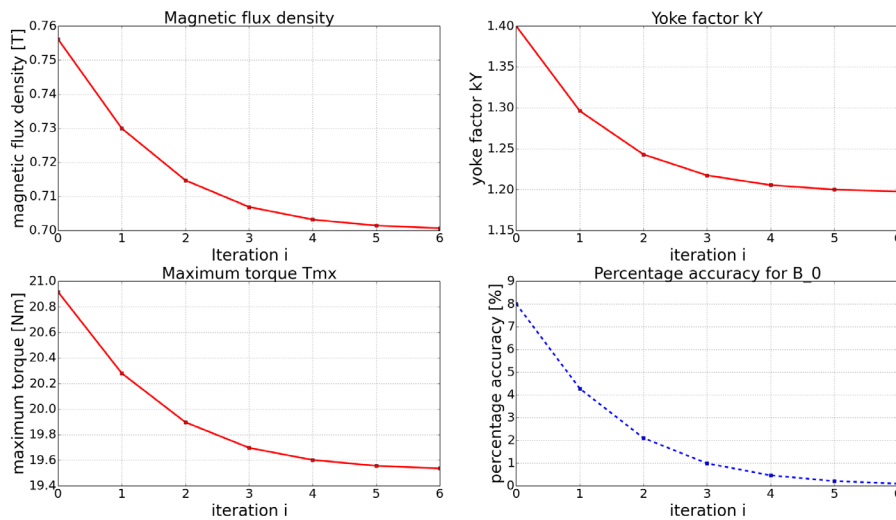


**Fig. 17.** Results: magnetic flux density $B_0$, yoke factor $k_Y$, clutching torque $T$, and percentage accuracy for $B_0$ for Variant 1, Case I ($k_Y = 1.4$)
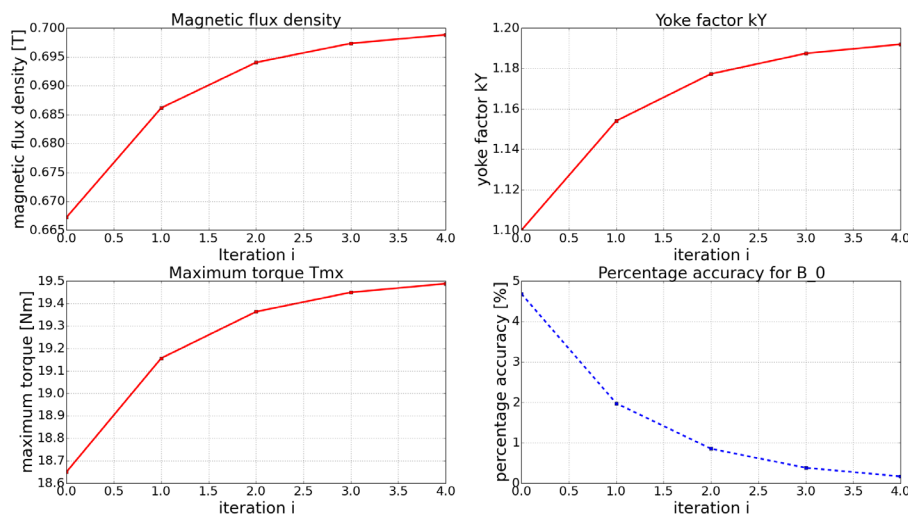


**Fig. 18.** Results: magnetic flux density $B_0$, yoke factor $k_Y$, clutching torque $T$, and percentage accuracy for $B_0$ for Variant 1, Case II ($k_Y = 1.1$)
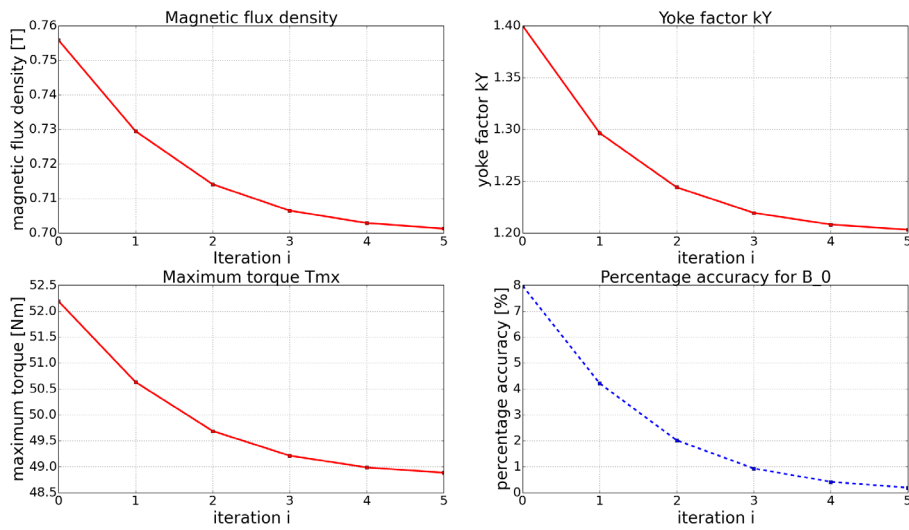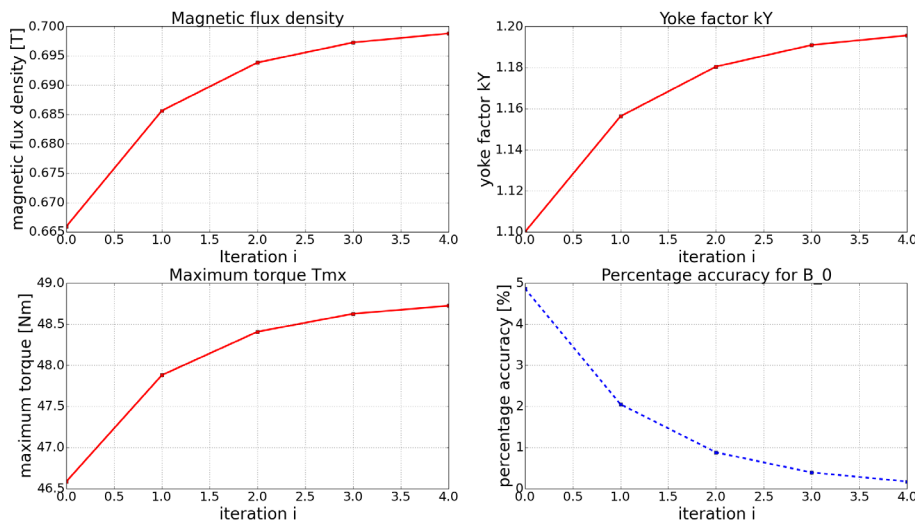
**Fig. 19.** Results: magnetic flux density $B_0$, yoke factor $k_Y$, clutching torque $T$, and percentage accuracy for $B_0$ for Variant 2, Case I ($k_Y = 1.4$)



**Fig. 20.** Results: magnetic flux density $B_0$, yoke factor $k_Y$, clutching torque $T$, and percentage accuracy for $B_0$ for Variant 2, Case II ($k_Y = 1.1$)

design procedure" (the last row in Tables 1–4) allows us to determine the above dimensions and data after 4–6 iterations with accuracies of (0.1–0.2)% for $B_0$ and (2.2–2.6)% for $T_{mx}$.

It should be noted that the proposed method allows to obtain the desired solution with a small number of iterations compared to other methods described in the literature. For example, in the method described in [10] the number of iterations was close to 40. The significant reduction in the number of iterations in the method proposed by the authors is reflected in a significant reduction in computational time. The results presented in Tables 1–4 and in the Figs. 17–20 were obtained in about 90 seconds (calculations were carried out on a laptop computer with the Intel core i5-8300H processor and 16GB RAM). For the methods presented in publications [7, 23] the computational time was much longer and ranged from several

minutes to several hours. The reduction of the number of iterations and the reduction of computational time in the proposed two-stage method is therefore its another significant advantage.

## 5. CONCLUSIONS

Based on experience and practice in designing electrical machines and other unconventional electromechanical convertors and devices (also with smart materials, such as MR fluid and SMA), the authors developed a new analytical-field design method for MR multi-disc clutches. This method includes an "Analytical stage of design procedure" (consisting of a series of only 36 algebraic expressions) and "Field stage of design procedure" based on the FEM calculations. The main advantage of the proposed method is in the harmonious combination of both

Bull. Pol. Acad. Sci. Tech. Sci. 69(6) 2021, e139392

13

stages, and clear physical and technical interpretation of all the relationships. The first analytical stage of the design procedure leads to a solution close to the assumed operational data with an accuracy of (4–8)%. The second field stage of this procedure enables us to refine this solution in only 4–6 iterations to the level of accuracy of 0.2% for $B_0$ and 2.6% for $T_{mx}$.

According to the authors, the essence of the new method is the introduction of a yoke factor $k_Y$, the concept of which is based on the theory of induction machines (analogous to the saturation factor determining the ratio of total MMF to MMF required for magnetising the air gap alone). The recommended initial value of the yoke factor $k_Y$ for the first analytical stage of the calculations ($i = 0$) is $k_Y = 1.1-1.2$.

Another important advantage of the method is its clear structure, which is characterised by the block diagram displayed in Fig. 13, and the breakdown of the results into outcomes "independent of yoke factor $k_Y$" and "dependent on yoke factor $k_Y$" (see Fig. 14). The elaborated design method also guarantees that the magnetic flux density at the most saturated point of the magnetic circuit (this point lies within the cover yoke at a length equal to approximately the sum $r_{Bmx} \cong r_{1e} + g$) is close to the assumed maximum value of $B_{mx}$ (this value was taken to be equal to $1.2T$, correspondingly less than the saturation magnetic flux density $1.6T$). The obtained results were $B_{mx} = 1.273T$ (Variant 1, Case I), $B_{mx} = 1.269T$ (Variant 1, Case II), $B_{mx} = 1.247T$ (Variant 2, Case I), and $B_{mx} = 1.242T$ (Variant 2, Case II).

Moreover, the elaborated method is valid for a one-disc MR clutch, which can be considered as an exceptional case. The method can also be easily adapted to other MR devices analysed in shear mode.

The simplicity of the developed design method predisposes it to be used in optimisation calculations.

Finally, it should be noted that a significant problem in ensuring the controllability of the coupling torque by the excitation current is the use of an appropriate control system with the PID controler. In the case of devices with MR fluids, there is also the problem of possible degradation of the properties of the fluid during prolonged or improper use. Regarding the MR clutch, this may refer to the excessively long running time of the clutch in case of slip. Determining the value of this unacceptable working time and the value of the permissible slip requires supplementing the developed clutch model with thermal calculations, as well as conducting experimental tests of the prototype focused on the analysis of the temperature field distribution [37].

## REFERENCES

[1] P. Martynowicz, "Study of vibration control using laboratory test rig of wind turbine tower-nacelle system with mr damper based tuned vibration absorber," *Bull. Pol. Acad. Sci. Tech. Sci.*, vol. 64, no. 2, pp. 347–359, 2016.

[2] J. Snamina and B. Sapiński, "Energy balance in self-powered mr damper-based vibration reduction system," *Bull. Pol. Acad. Sci. Tech. Sci.*, vol. 59, no. 1, pp. 75–80, 2011, doi: 10.2478/v10175-011-0011-4.

[3] J.L.U. Lee, A.K. Saha *et al.*, "Design and performance evaluation of a rotary magnetorheological damper for unmanned vehicle suspension systems," *Sci. World J.*, 2013, doi: 10.1155/2013/894016.

[4] A. Pręgowska, R. Konowrocki, and T. Szolc, "On the semi-active control method for torsional vibrations in electro-mechanical systems by means of rotary actuators with a magneto-rheological fluid," *J. Theor. Appl. Mech.*, vol. 51, no. 4, pp. 979–992, 2013.

[5] J. Gołdasz and B. Sapiński, *Insight into Magnetorheological Shock Absorbers*, ser. EBL-Schweitzer. Springer International Publishing, 2014. [Online]. Available: https://books.google.pl/books?id=CbXzBQAAQBAJ.

[6] W. East, J. Turcotte, J.-S. Plante, and G. Julio, "Experimental assessment of a linear actuator driven by magnetorheological clutches for automotive active suspensions," *J. Intell. Mater. Syst. Struct.*, vol. 32, no. 9, p. 955–970, 2021, doi: 10.1177/1045389X21991237.

[7] E.J. Park, L. Falcao, and A. Suleman, "Multidisciplinary design optimization of an automotive magnetorheological brake design," *Comput. Struct.*, vol. 28, pp. 207–216, 2008, doi: 10.1016/j.compstruc.2007.01.035.

[8] C. Rossa, A. Jaegy, A. Micaelli, and J. Lozada, "Development of a multilayered wide-ranged torque magnetorheological brake," *Smart Mater. Struct.*, vol. 23, no. 2, p. 025028, Jan 2014, doi: 10.1088/0964-1726/23/2/025028.

[9] C. Rossa, A. Jaegy, J. Lozada, and A. Micaelli, "Design considerations for magnetorheological brakes," *IEEE/ASME Trans. Mechatron.*, vol. 19, no. 5, pp. 1669–1680, 2014, doi: 10.1109/TMECH.2013.2291966.

[10] J.W. Sohn, J. Jeon, Q.H. Nguyen, and S.-B. Choi, "Optimal design of disc-type magneto-rheological brake for mid-sized motorcycle: experimental evaluation," *Smart Mater. Struct.*, vol. 24, no. 8, p. 085009, Jul 2015, doi: 10.1088/0964-1726/24/8/085009.

[11] S. Li, W. Meng, and Y. Wang, "Numerical and experimental studies on a novel magneto-rheological fluid brake based on fluid–solid coupling," *Sci. Prog.*, vol. 103, no. 1, p. 0036850419879000, 2020, doi: 10.1177/0036850419879000.

[12] K. Kluszczyński and Z. Pilch, "Mr multi disc clutches – construction, parameters and field model," in *2019 20th International Conference on Research and Education in Mechatronics (REM)*, May 2019, pp. 1–6, doi: 10.1109/REM.2019.8744131.

[13] H. Böse, T. Gerlach, and J. Ehrlich, "Magnetorheological torque transmission devices with permanent magnets," *J. Phys. Conf. Ser.*, vol. 412, p. 012050, Feb 2013, doi: 10.1088/1742-6596/412/1/012050.

[14] F. Bucchi, P. Forte, F. Frendo, A. Musolino, and R. Rizzo, "A fail-safe magnetorheological clutch excited by permanent magnets for the disengagement of automotive auxiliaries," *J. Intell. Mater. Syst. Struct.*, vol. 25, no. 16, pp. 2102–2114, 2014, doi: 10.1177/1045389X13517313.

[15] Z. Li, X. Zhang, K. Guo, M. Ahmadian, and Y. Liu, "A novel squeeze mode based magnetorheological valve: design, test and evaluation," *Smart Mater. Struct.*, vol. 25, no. 12, p. 127003, Nov 2016, doi: 10.1088/0964-1726/25/12/127003.

[16] Z. Pilch and J. Domin, "Conception of the throttle-return valve for the magnetorheological fluid," *Arch. Electr. Eng.*, vol. 67, no. 1, 2018, doi: 10.24425/118990.

[17] B. Horváth and I. Szalai, "Nonlinear magnetic properties of magnetic fluids for automotive applications," *Hung. J. Ind. Chem.*, vol. 48, no. 1, p. 61–65, Jul 2020, doi: 10.33927/hjic-2020-09.

14

Bull. Pol. Acad. Sci. Tech. Sci. 69(6) 2021, e139392

[18] P. Kowol and Z. Pilch, "Analysis of the magnetorheological clutch working at full slip state," *Electr. Rev.*, vol. R. 91, no. 6, pp. 108–111, 2015.

[19] G. Chen, Y. Lou, and T. Shang, "Mathematic modeling and optimal design of a magneto-rheological clutch for the compliant actuator in physical robot interactions," *IEEE Rob. Autom. Lett.*, vol. 4, no. 4, pp. 3625–3632, 2019, doi: 10.1109/LRA.2019.2928766.

[20] R. Rizzo, "An innovative multi-gap clutch based on magnetorheological fluids and electrodynamic effects: magnetic design and experimental characterization," *Smart Mater. Struct.*, vol. 26, no. 1, p. 015007, Dec 2016, doi: 10.1088/0964-1726/26/1/015007.

[21] Q.H. Nguyen and S.B. Choi, "Selection of magnetorheological brake types via optimal design considering maximum torque and constrained volume," *Smart Mater. Struct.*, vol. 21, no. 1, p. 015012, Dec 2011, doi: 10.1088/0964-1726/21/1/015012.

[22] W. Burlikowski and K. Kluszczyński, "Comparison of different mathematical models of an electromechanical actuator," in *2012 9th France-Japan 7th Europe-Asia Congress on Mechatronics (MECATRONICS)/13th Int'l Workshop on Research and Education in Mechatronics (REM)*, 2012, pp. 403–408.

[23] P.-B. Nguyen and S.-B. Choi, "A new approach to magnetic circuit analysis and its application to the optimal design of a bi-directional magnetorheological brake," *Smart Mater. Struct.*, vol. 20, no. 12, p. 125003, Nov 2011, doi: 10.1088/0964-1726/20/12/125003.

[24] T. Wolnik, "Alternate computational method for induction disk motor based on 2d fem model of cylindrical motor," *Arch. Electr. Eng.*, vol. 69, no. 2020, pp. 233–244, 2020, doi: 10.24425/aee.2020.131770.

[25] P. Kowol, "Application of magnetic field model for design procedure of magnetorheological rotary-linear brake," *Electr. Rev.*, vol. 81, no. 12, pp. 22–24, 2005.

[26] M. Kciuk, K. Chwastek, K. Kluszczyński, and J. Szczygłowski, "A study on hysteresis behaviour of sma linear actuators based on unipolar sigmoid and hyperbolic tangent functions," Sens. Actuators, A, vol. 243, pp. 52–58, 2016, doi: 10.1016/j.sna.2016.02.012.

[27] M. Kciuk, W. Kuchcik, Z. Pilch, and W. Klein, "A novel sma drive based on the Graham Clock escapement and resistance feedback," *Sens. Actuators, A*, vol. 285, pp. 406–413, 2019, doi: 10.1016/j.sna.2018.11.044.

[28] B.W. Inc., "bearing-sizes." [Online]. Available: https://www.bearingworks.com/bearing-sizes/.

[29] LORD-CORPORATION, "Mrf-140cgmrfluid." [Online]. Available: https://lordfulfillment.com/pdf/44/DS7012_MRF-140CG-MRFluid.pdf.

[30] A. Suite. [Online]. Available: http://www.agros2d.org/.

[31] V. Hegde and G. Maruthi, "Experimental investigation on detection of air gap eccentricity in induction motors by current and vibration signature analysis using non-invasive sensors," *Energy Procedia*, vol. 14, pp. 1047–1052, 2012, 2011 2nd International Conference on Advances in Energy Engineering (ICAEE).

[32] X. Hu, Y. Li, and L. Luo, "The influence of air gap thickness between the stator and rotor on nuclear main pump," *Energy Procedia–Proceedings of the 9th International Conference on Applied Energy*, vol. 142, pp. 259–264, 2017, doi: 10.1016/j.egypro.2017.12.041.

[33] M.N. Benallal, M.A. Vaganov, D.S. Pantouhov, E. Ailam, and K. Hamouda, "Optimal value of air gap induction in an induction motor," in *The XIX International Conference on Electrical Machines – ICEM 2010*, 2010, pp. 1–4, doi: 10.1109/ICELMACH.2010.5608185.

[34] K. Kluszczyński and Z. Pilch, "Basic features of mr clutches – resulting from different number of discs," in *2019 15th Selected Issues of Electrical Engineering and Electronics (WZEE)*, December 2019, pp. 1–4, doi: 10.1109/WZEE48932.2019.8979786.

[35] J.H. Kuhlmann, *Design of electrical apparatus*. New York, J. Wiley and Sons; London, Chapman and Hall, 1954.

[36] ASTM International, "Standard specification for standard nominal diameters and cross-sectional areas of AWG sizes of solid round wires used as electrical conductors," 2014. [Online]. Available: http://www.astm.org/Standards/B258.htm.

[37] J. Bajkowski, "Operational characteristics of rotating magnetorheological clutches and brakes," *J. Mach. Constr. Maint.*, vol. 106, no. 3/2017, pp. 7–12, 2017.